Euro. Jnl of Applied Mathematics (2020), *vol.* 31, *pp.* 553–573 © Cambridge University Press 2019.
doi:10.1017/S0956792519000160

Scattering coefficients of inhomogeneous objects and their application in target classification in wave imaging

LORENZO BALDASSARI

Department of Mathematics, ETH Zürich, Rämistrasse 101, CH-8093 Zürich, Switzerland
e-mail: lorenzo.baldassari@sam.math.ethz.ch

(*Received 8 July 2018*; *revised 18 February 2019*; *accepted 6 June 2019*; *first published online 3 July 2019*)

The aim of this paper is to provide and numerically test in the presence of measurement noise a procedure for target classification in wave imaging based on comparing frequency-dependent distribution descriptors with precomputed ones in a dictionary of learned distributions. Distribution descriptors for inhomogeneous objects are obtained from the scattering coefficients. First, we extract the scattering coefficients of the (inhomogeneous) target from the perturbation of the reflected waves. Then, for a collection of inhomogeneous targets, we build a frequency-dependent dictionary of distribution descriptors and use a matching algorithm in order to identify a target from the dictionary up to some translation, rotation and scaling.

Key words: Target classification, inhomogeneous inclusions, scattering coefficients, frequency-dependent distribution descriptors, Far-field measurements

2010 Mathematics Subject Classification: Primary: 65N21. Secondary: 35R30; 35B30; 65Z05.

1 Introduction

There are several geometric and physical quantities associated with target classification such as eigenvalues and capacities [21]. The concept of scattering coefficients is one of them. The notion of scattering coefficients was introduced for the first time for homogeneous electromagnetic inclusions in order to enhance near cloak invisibility [13, 14]. They have been used by Ammari *et al.* for inverse medium scattering [5], echo-sensing [15, 22, 23] and mathematical analysis of super-resolution phenomena in imaging [8]. Recently, scattering coefficients have been used for phaseless domain reconstruction [7] and to study the scattering and absorption enhancements by plasmon resonant nanoparticles [17]. The notion of scattering coefficients of an elastic inclusion was also investigated in [1]. Scattering coefficients are frequency-dependent objects. In electromagnetic and acoustic media, they provide a natural extension of the concept of polarisation tensors [10, 11, 16] with respect to frequency dependence. In target classification in wave imaging, scattering coefficients play the same role as the contracted generalised polarisation tensors (CGPTs) for the conductivity equation [3, 10]. As CGPTs, scattering coefficients are useful to recognise targets with constitutive electromagnetic parameters different from those of the background medium. As far as we know, scattering coefficients have been successfully applied to classify homogeneous targets only [15]. Therefore, it is natural to ask the question whether the notion of scattering coefficients can be applied successfully also to targets with inhomogeneous electromagnetic parameters.

https://doi.org/10.1017/S0956792519000160 Published online by Cambridge University Press

To mathematically introduce the concept of the scattering coefficients in wave imaging, we consider the Helmholtz problem in $\mathbb{R}^2$ for a given fixed frequency $\omega > 0$:

$$\begin{cases} \nabla \cdot (\chi(\mathbb{R}^2 \setminus \bar{B}) + \frac{1}{\sigma}\chi(B))\nabla u + \omega^2(\chi(\mathbb{R}^2 \setminus \bar{B}) + \mu\chi(B))u = 0 & \text{in } \mathbb{R}^2, \\ \left| \frac{\partial(u-U)}{\partial|x|} - i\omega(u-U) \right| \leq \frac{K}{|x|^{\frac{3}{2}}} & \text{if } |x| \to \infty. \end{cases} \tag{1.1}$$

Here, K is a positive constant, B is the target embedded in $\mathbb{R}^2$ with Lipschitz boundary, $\chi(B)$ (resp. $\chi(\mathbb{R}^2 \setminus \bar{B})$) is the characteristic function of B (resp. $\mathbb{R}^2 \setminus \bar{B}$), the positive constants σ and μ are the magnetic permeability and electric permittivity of the target, which are supposed to be different from the background permittivity and permeability (the constant function 1), U is the background solution, that is, a given solution to $(\Delta + \omega^2)U = 0$ and the (weak) solution u to (1.1) represents the perturbed wave. The perturbation $u - U$ due to the presence of target B admits the following asymptotic expansion as $|x| \to \infty$, see [15]:

$$u(x) - U(x) = -\frac{i}{4} \sum_{n\in\mathbb{Z}} H_n^{(1)}(\omega|x|)e^{in\theta_x} \sum_{m\in\mathbb{Z}} W_{n,m}[B, \sigma, \mu, \omega]a_m(U), \tag{1.2}$$

where $H_n^{(1)}$ are the Hankel functions of the first kind of order n and $a_m(U)$ are constants such that $U(x) = \sum_{m\in\mathbb{Z}} a_m(U)J_m(\omega|x|)e^{im\theta_x}$ with J_m being the Bessel function of order m. The building blocks $W_{n,m}[B, \sigma, \mu, \omega]$ for the asymptotic expansion (1.2) are called the scattering coefficients [13, 15].

This paper extends the results of [15] to targets with inhomogeneous permittivities and permeabilities. The concept of inhomogeneous scattering coefficients was first introduced by Ammari *et al.* in [5] and used later in [8] to prove resolution enhancement in high-contrast media. It is the purpose of this paper to study for the first time the application of the inhomogeneous scattering coefficients in target classification. For a collection of inhomogeneous targets, we use the scattering coefficients to build a frequency-dependent dictionary of precomputed distribution descriptors which are invariant to rigid transformations. To derive the distribution descriptors, it is important to introduce such properties of the scattering coefficients as translation, rotation and scaling formula. Finally, we use a target identification algorithm in order to identify an inhomogeneous target from the dictionary of precomputed distribution descriptors up to some translation, rotation and scaling. Note that all numerical tests are performed in the presence of measurement noise. The main result of this paper is a complete scheme which depicts the probability of recognition for the inhomogeneous targets of the dictionary at different noise levels. For the sake of simplicity, throughout this paper, we focus on two-dimensional models. However, the results can be easily extended to three dimensions.

The paper is organised as follows. In Section 2 we introduce the problem formulation. In Section 3 we review the concept of inhomogeneous scattering coefficients. We also derive a full far-field expansion of $(u - U)(x)$ as $|x| \to \infty$ in terms of the inhomogeneous scattering coefficients. This will be useful in view of the numerical tests of Section 5. In fact, the scattering coefficients $W_{n,m}[B, \sigma, \mu, \omega]$ of the unknown targets can be reconstructed from the far-field expansion of u by a least-squared method [15]. In Section 4 we construct the translation- and rotation-invariant distribution descriptor. Finally, in Section 5 we use the theoretical framework presented in previous sections in order to prove the applicability of [15] to inhomogeneous targets. A variety of numerical results are shown, including a figure showing the probability of recognition for all targets of the dictionary at different noise levels. A few concluding remarks

https://doi.org/10.1017/S0956792519000160 Published online by Cambridge University Press

are given in Section 6. In Appendix, we present detailed results of target identification using a full-view setting with no noise ($\sigma_0 = 0\%$).

2 Problem formulation

Let $\frac{1}{\sigma}$ be a bounded measurable function in $\mathbb{R}^2$ such that $\frac{1}{\sigma} - 1$ is compactly supported and

$$0 < \lambda_1 \leq \frac{1}{\sigma} \leq \lambda_2,$$

where λ_1, λ_2 are constants. Let μ be a bounded measurable function in $\mathbb{R}^2$ such that $\mu - 1$ is compactly supported and

$$0 < \lambda_3 \leq \mu \leq \lambda_4,$$

where λ_3, λ_4 are constants. For a given fixed frequency $\omega > 0$, let u be the (weak) solution to the following Helmholtz problem:

$$\begin{cases} \nabla \cdot \frac{1}{\sigma} \nabla u + \omega^2 \mu u = 0 & \text{in } \mathbb{R}^2, \\ \left| \frac{\partial (u-U)}{\partial |x|} - i\omega(u-U) \right| \leq \frac{K}{|x|^{\frac{3}{2}}} & \text{if } |x| \to \infty, \end{cases} \tag{2.1}$$

where U is a given solution to

$$\Delta U + \omega^2 U = 0, \tag{2.2}$$

and $|\cdot|$ denotes the Euclidean norm of $\mathbb{R}^2$.

2.1 The Helmholtz equation

Let B a bounded domain in $\mathbb{R}^2$ with Lipschitz boundary. We assume that B is such that

$$\operatorname{supp}\left(\frac{1}{\sigma} - 1\right) \subset B,$$

$$\operatorname{supp}(\mu - 1) \subset B.$$

Suppose that B contains the origin. Note that (2.1) is equivalent to

$$\begin{cases} \nabla \cdot \frac{1}{\sigma} \nabla u + \omega^2 \mu u = 0 & \text{in } B, \\ \Delta u + \omega^2 u = 0 & \text{in } \mathbb{R}^2 \setminus \bar{B}, \\ u|_+ - u|_- = 0 & \text{on } \partial B, \\ \nu \cdot \nabla u|_+ - \nu \cdot \frac{1}{\sigma} \nabla u|_- = 0 & \text{on } \partial B, \\ \left| \frac{\partial (u-U)}{\partial |x|} - i\omega(u-U) \right| \leq \frac{K}{|x|^{\frac{3}{2}}} & \text{if } |x| \to \infty, \end{cases} \tag{2.3}$$

where ν is the outward normal vector at some $x \in \partial B$ and the subscripts $\pm$ indicate the limits from outside and inside B, respectively.

In two dimensions, the fundamental solution $\Gamma_\omega(x)$ to the Helmholtz equation

$$(\Delta + \omega^2)\Gamma_\omega(x) = \delta_0(x)$$

https://doi.org/10.1017/S0956792519000160 Published online by Cambridge University Press

subject to the Sommerfeld outgoing radiation condition is given by

$$\Gamma_\omega(x) = -\frac{i}{4}H_0^{(1)}(\omega|x|).$$

Assume that ω^2 is not a Neumann eigenvalue of $-\frac{1}{\mu(x)}\nabla\cdot\frac{1}{\sigma(x)}\nabla$ on B. Let $N_{\sigma,\mu}$ be the Neumann function of problem

$$\begin{cases} \nabla\cdot\frac{1}{\sigma}\nabla u + \omega^2\mu u = 0 & x\in B,\\ \frac{1}{\sigma}\frac{\partial u}{\partial \nu} = g & x\in\partial B, \end{cases} \tag{2.4}$$

that is, for each fixed $z\in B$, $N_{\sigma,\mu}(\cdot,z)$ is solution to

$$\begin{cases} \nabla_x\cdot\frac{1}{\sigma(x)}\nabla_x N_{\sigma,\mu}(x,z) + \omega^2\mu(x)N_{\sigma,\mu}(x,z) = -\delta_z(x) & x\in B,\\ \frac{1}{\sigma(x)}\nabla_x N_{\sigma,\mu}(x,z)\nu_x = 0 & x\in\partial B. \end{cases} \tag{2.5}$$

Note that $N_{\sigma,\mu}(x,z)$ is defined as a function of $x\in\bar{B}$ for each fixed $z\in B$. The function defined by

$$\mathcal{N}_{B,\sigma,\mu}[g](z) := \int_{\partial B} N_{\sigma,\mu}(x,z)g(x)\,dS_x,\ \ z\in B, \tag{2.6}$$

is the solution to (2.4). Moreover, the Neumann-to-Dirichlet (NtD) map $\Lambda_{\sigma,\mu}: H^{-\frac{1}{2}}(\partial B)\to H^{\frac{1}{2}}(\partial B)$ is well defined, invertible and

$$\Lambda_{\sigma,\mu}[g](z) = \mathcal{N}_{B,\sigma,\mu}[g]\big|_{\partial B}(z) = u|_{\partial B}(z),$$

where $\mathcal{N}_{B,\sigma,\mu}[g]$ is well defined on ∂B since the Neumann function $N_{\sigma,\mu}(x,z)$ has the same singularity type of $\Gamma_\omega(|x-z|)$ as $|x-z|\to 0$ (see Appendix of [5]; for a more detailed analysis, see [6, 12]).

2.2 Layer potentials and representation of the solution

We introduce the single-layer potential and the trace operator as follows: the single-layer potential and the trace operator are given by

$$S_B^\omega[\phi](x) = \int_{\partial B}\Gamma_\omega(x-y)\phi(y)\,dS_y,$$

and

$$(K_B^\omega)^*[\phi](x) = \int_{\partial B}\frac{\partial\Gamma_\omega}{\partial\nu_x}(x-y)\phi(y)\,dS_y,$$

where $\phi\in L^2(\partial B)$. The following jump formula holds:

$$\frac{\partial S_B^\omega[\phi]}{\partial\nu}\bigg|_\pm(x) = \left(\pm\frac{1}{2}I + (K_B^\omega)^*\right)[\phi](x)\ \text{ a.e. } x\in\partial B,$$

where $f|_+$ and $f|_-$ denote, respectively, the limit on ∂B from the outside and the inside of B along the normal direction, and $\partial/\partial\nu$ denotes the normal derivative. We now recall from [5] the main result that will allow us to represent the solution u to (2.1) through layer potentials.

https://doi.org/10.1017/S0956792519000160 Published online by Cambridge University Press

Lemma 2.1 *Define the operator* $A : L^2(\partial B) \times L^2(\partial B) \to L^2(\partial B) \times L^2(\partial B)$ *as*

$$A := \begin{pmatrix} -S_B^\omega & \Lambda_{\sigma,\mu} \\ -\left(\frac{1}{2}I + (K_B^\omega)^*\right) & I \end{pmatrix}.$$

If ω^2 *is not a Dirichlet eigenvalue of* $-\Delta$ *on* B, A *is invertible.*

Then the following system admits a unique solution $(\phi, \psi) \in L^2(\partial B) \times L^2(\partial B)$:

$$\begin{cases} U(x) + S_B^\omega[\phi](x) = \Lambda_{\sigma,\mu}[\psi](x), \\ \psi(x) = \left(\frac{1}{2}I + (K_B^\omega)^*\right)[\phi](x) + \frac{\partial U}{\partial \nu}(x), \end{cases} \quad x \in \partial B, \tag{2.7}$$

provided that ω^2 is not a Dirichlet eigenvalue of $-\Delta$ on B. The solution u to (2.1) may be represented through layer potentials as

$$u(x) = \begin{cases} U(x) + S_B^\omega[\phi](x) & x \in \mathbb{R}^2 \setminus \bar{B}, \\ \mathcal{N}_{B,\sigma,\mu}[\psi](x) & x \in B. \end{cases} \tag{2.8}$$

3 Scattering coefficients and asymptotic expansion

In the following, we use $\mathcal{C}_m$ to denote the cylindrical wave of index $m \in \mathbb{Z}$ and of wave number ω, which is defined by

$$\mathcal{C}_m(y) = \mathcal{C}_{m,\omega}(y) := J_m(\omega|y|)e^{im\theta_y}, \tag{3.1}$$

where J_n is the Bessel function of the first kind of order n. Since the family of cylindrical waves $(\mathcal{C}_m(x))_m$ is complete [10], the source term U solution to (2.2) admits the following expansion:

$$U(x) = \sum_{m\in\mathbb{Z}} a_m(U)\mathcal{C}_m(x),$$

where $a_m(U)$ are constants. Since (2.7) is linear, we get

$$\psi(x) = \sum_{m\in\mathbb{Z}} a_m(U)\psi_m(x),$$

and

$$\phi(x) = \sum_{m\in\mathbb{Z}} a_m(U)\phi_m(x).$$

We introduce the inhomogeneous scattering coefficients as follows [5].

Definition 3.1 For $m \in \mathbb{Z}$, let $(\phi_m, \psi_m) \in L^2(\partial B) \times L^2(\partial B)$ be the solution to (2.7) with the cylindrical wave $\mathcal{C}_m$ as the source term U. For $n \in \mathbb{Z}$, we define the scattering coefficients associated with the permittivity and permeability distributions $\mu(x)$, $\sigma(x)$ and the frequency $\omega > 0$ as follows:

$$W_{n,m} = W_{n,m}[B, \sigma, \mu, \omega] = \int_{\partial B} \overline{\mathcal{C}_n(y)}\phi_m(y)\, dS_y. \tag{3.2}$$

https://doi.org/10.1017/S0956792519000160 Published online by Cambridge University Press

For $|x| > |y|$, by Graf's addition formula [2],

$$\Gamma_\omega(x-y) = -\frac{i}{4}\sum_{n\in\mathbb{Z}} H_n^{(1)}(\omega|x|)e^{in\theta_x}\overline{\mathcal{C}_n(y)},$$

where $x = (|x|, \theta_x)$, $y = (|y|, \theta_y)$ and $H_n^{(1)}$ is the Hankel function of the first kind of order n. The solution u to (2.1) admits the following asymptotic expansion as $|x| \to \infty$:

$$(u-U)(x) = -\frac{i}{4}\sum_{n\in\mathbb{Z}} H_n^{(1)}(\omega|x|)e^{in\theta_x} a_m(U) W_{n,m}[B,\sigma,\mu,\omega]. \tag{3.3}$$

Note that expansion (3.3) is useful in view of Section 5 since it shows that the inhomogeneous scattering coefficients $W_{n,m}$ of an unknown target can be reconstructed from the far-field measurement of $u - U$ by a least-square method.

4 Distribution descriptors and identification in a dictionary

In this section, we construct the distribution descriptors which are invariant to rigid transformations. We extend the results of [15]. In the following, we denote by B a reference shape of size 1 centred at the origin, so that the unknown target D is generated from B by a rotation with angle θ, a scaling $s > 0$ and a translation $z \in \mathbb{R}^2$ as

$$D = z + sR_\theta B.$$

4.1 Transformation formulas of the scattering coefficients

We introduce the notation for translation, scaling and rotation of a shape B as

$$B^z := B + z,\ B^s := sB,\ B^\theta = e^{i\theta}B,$$

and those of the material parameter σ (resp. μ) as

$$\sigma^z := \sigma(\cdot - z),\ \sigma^s := \sigma(s^{-1}\cdot),\ \sigma^\theta := \sigma(e^{-i\theta}\cdot).$$

We denote by $\phi_{U,B} = \phi_{U,B,\omega}$ the solution to (2.7) given the domain B, the source term U and the frequency ω.

There exist explicit relations between the inhomogeneous scattering coefficients of B and B^z, B^s, B^θ. By deriving them, we can define the translation- and rotation-invariant distribution descriptors that occur in the target identification procedure of Section 5. The following Proposition was proved in [5].

Proposition 4.1 (Transformation formulas) *For any $z \in \mathbb{R}^2$, $s > 0$ and θ, the following relation holds:*

(a) $W_{n,m}[B^z,\sigma^z,\mu^z,\omega] = \sum_{a,b}\overline{\mathcal{C}_a(z)}\mathcal{C}_b(z)W_{n-a,m-b}[B,\sigma,\mu,\omega]$.
(b) $W_{n,m}[B^s,\sigma^s,\mu^s,\omega] = W_{n,m}[B,\sigma,\mu,s\omega]$.
(c) $W_{n,m}[B^\theta,\sigma^\theta,\mu^\theta,\omega] = e^{i(m-n)\theta}W_{n,m}[B,\sigma,\mu,\omega]$.

https://doi.org/10.1017/S0956792519000160 Published online by Cambridge University Press

4.2 Far-field pattern and scattering coefficients

To construct the distribution descriptors which are invariant to rigid transformations, we derive the far-field pattern of the scattering field in terms of the inhomogeneous scattering coefficients.

If U is given by a plane wave $e^{i\omega\xi\cdot x}$ such that $\omega\xi\cdot\omega\xi=\omega^2$, then by the Jacobi–Anger decomposition, we have

$$U(x)=\sum_{m\in\mathbb{Z}} e^{im(\frac{\pi}{2}-\theta_\xi)}J_m(\omega|x|)e^{im\theta_x}=\sum_{m\in Z} e^{im(\frac{\pi}{2}-\theta_\xi)}\mathcal{C}_m(x).$$

By the linearity of (2.7), we obtain

$$\phi=\sum_{m\in\mathbb{Z}} e^{im(\frac{\pi}{2}-\theta_\xi)}\phi_m.$$

Using (3.3),

$$u-e^{i\omega\xi\cdot x}=(u-U)(x)=-\frac{i}{4}\sum_{m\in\mathbb{Z}} e^{im(\frac{\pi}{2}-\theta_\xi)}\int_{\partial B} H_0^{(1)}(\omega|x-y|)\phi_m(y)\,dS_y. \tag{4.1}$$

Recall that [2]

$$H_0^{(1)}(\omega|x-y|)=\sqrt{\frac{2}{\pi\omega|x-y|}}e^{i(\omega|x-y|-\frac{\pi}{4})}+O(|x|^{-1}) \text{ as } |x|\to\infty.$$

Since $|x-y|=|x|-|y|\cos(\theta_x-\theta_y)+O(|x|^{-1})$, (4.1) becomes

$$u-e^{i\omega\xi\cdot x}=-ie^{-i\frac{\pi}{4}}\frac{e^{i\omega|x|}}{\sqrt{8\pi\omega|x|}}\sum_{m\in\mathbb{Z}} e^{im(\frac{\pi}{2}-\theta_\xi)}\int_{\partial B} e^{-i\omega|y|\cos(\theta_x-\theta_y)}\phi_m(y)\,dS_y+O(|x|^{-1}). \tag{4.2}$$

By Jacobi–Anger identity,

$$e^{-i\omega|y|\cos(\theta_x-\theta_y)}=e^{i\omega|y|\cos(\theta_x-\theta_y+\pi)}=\sum_{n\in\mathbb{Z}} i^nJ_n(\omega|y|)e^{in(\theta_x-\theta_y+\pi)},$$

(4.2) becomes

$$u-e^{i\omega\xi\cdot x}=-ie^{-i\frac{\pi}{4}}\frac{e^{i\omega|x|}}{\sqrt{8\pi\omega|x|}}\sum_{m,n\in\mathbb{Z}} e^{im(\frac{\pi}{2}-\theta_\xi)}e^{in(\theta_x-\frac{\pi}{2})}\int_{\partial B} i^nJ_n(\omega|y|)e^{-in(\theta_y-\frac{3}{2}\pi)}\phi_m(y)\,dS_y+O(|x|^{-1}). \tag{4.3}$$

Since $i^ne^{in\frac{3\pi}{2}}=i^n(-i)^n=1$, we obtain

$$u-e^{i\omega\xi\cdot x}=-ie^{-i\frac{\pi}{4}}\frac{e^{i\omega|x|}}{\sqrt{8\pi\omega|x|}}\sum_{m,n\in\mathbb{Z}} e^{im(\frac{\pi}{2}-\theta_\xi)}e^{in(\theta_x-\frac{\pi}{2})}W_{n,m}+O(|x|^{-1}), \tag{4.4}$$

where $W_{n,m}$ are the inhomogeneous scattering coefficients.

We define the far-field pattern (the scattering amplitude) when the incident field is the plane wave $U(x)=e^{i\omega\xi\cdot x}$, $|\xi|=1$, as the two-dimensional 2π-periodic function

$$A_B^\infty((\theta_\xi,\theta_x)^T;\sigma,\mu,\omega)=\sum_{m\in\mathbb{Z}} e^{im(\frac{\pi}{2}-\theta_\xi)}\int_{\partial B} e^{-i\omega|y|\cos(\theta_x-\theta_y)}\phi_m(y)\,dS_y.$$

From (4.4), we get the following proposition.

https://doi.org/10.1017/S0956792519000160 Published online by Cambridge University Press

Proposition 4.2 *Let* $(\theta_\xi, \theta_x)^T \in [0, 2\pi]^2$. *Then, we have*

$$A_B^\infty((\theta_\xi, \theta_x)^T; \sigma, \mu, \omega) = \sum_{m,n\in\mathbb{Z}} e^{im(\frac{\pi}{2}-\theta_\xi)} e^{in(\theta_x-\frac{\pi}{2})} W_{n,m}[B, \sigma, \mu, \omega]. \tag{4.5}$$

4.3 Translation- and rotation-invariant distribution descriptors

A simple relation exists between far-field patterns of $D = z + sR_\theta B$ and B. The following result generalises to the inhomogeneous case the result proved in [15] in the case of homogeneous scattering coefficients.

Proposition 4.3 *Let* $D = z + sR_\theta B$. *We denote by* θ_z *the angle of* z *in polar coordinates, and define*

$$\phi_z((\theta_\xi, \theta_x)^T) := e^{i\omega|z|\cos(\theta_\xi-\theta_z)} e^{-i\omega|z|\cos(\theta_x-\theta_z)}.$$

Then, we have

$$A_D^\infty((\theta_\xi, \theta_x)^T; \sigma, \mu, \omega) = \phi_z((\theta_\xi, \theta_x)^T) A_B^\infty((\theta_\xi - \theta, \theta_x - \theta)^T, \sigma, \mu, s\omega).$$

Proof By the transformation formulas of Proposition 4.1, we have

$$\begin{aligned} W_{n,m}[D, \sigma, \mu, \omega] &= \sum_{a,b\in\mathbb{Z}} \overline{\mathcal{C}_a(z)} \mathcal{C}_b(z) W_{n-a,m-b}[sR_\theta B, \sigma, \mu, \omega] \\ &= \sum_{a,b\in\mathbb{Z}} \overline{\mathcal{C}_a(z)} \mathcal{C}_b(z) W_{n-a,m-b}[R_\theta B, \sigma, \mu, s\omega] \\ &= \sum_{a,b\in\mathbb{Z}} \overline{\mathcal{C}_a(z)} \mathcal{C}_b(z) e^{i(m-b)\theta} e^{-i(n-a)\theta} W_{n-a,m-b}[B, \sigma, \mu, s\omega]. \end{aligned} \tag{4.6}$$

Therefore, using the Jacobi–Anger identity,

$$\begin{aligned} e^{i\omega|z|\cos(\theta_\xi-\theta_z)} = e^{i\omega|z|\cos(\theta_z-\theta_\xi)} &= \sum_{a\in\mathbb{Z}} i^a J_a(\omega|z|) e^{ia(\theta_z-\theta_\xi)} = \sum_{a\in\mathbb{Z}} J_a(\omega|z|) e^{ia(\frac{\pi}{2}-(\theta_\xi-\theta_z))} \\ &= \sum_{a\in\mathbb{Z}} \mathcal{C}_a(z) e^{ia(\frac{\pi}{2}-\theta_\xi)}, \end{aligned}$$

we obtain

$$\begin{aligned} A_D^\infty((\theta_\xi, \theta_x)^T; \sigma, \mu, \omega) &= \sum_{m,n\in\mathbb{Z}} e^{im(\frac{\pi}{2}-\theta_\xi)} e^{in(\theta_x-\frac{\pi}{2})} W_{n,m}[D, \sigma, \mu, \omega] \\ &= \sum_{m,n,a,b\in\mathbb{Z}} e^{im(\frac{\pi}{2}-\theta_\xi)} e^{in(\theta_x-\frac{\pi}{2})} \overline{\mathcal{C}_a(z)} \mathcal{C}_b(z) e^{i(m-b)\theta} e^{-i(n-a)\theta} W_{n-a,m-b}[B, \sigma, \mu, s\omega] \\ &= \sum_{m,n,a,b\in\mathbb{Z}} \overline{\mathcal{C}_a(z)} e^{-ia(\frac{\pi}{2}-\theta_x)} e^{ia(\frac{\pi}{2}-\theta_x)} \mathcal{C}_b(z) e^{im(\frac{\pi}{2}-\theta_\xi)} e^{in(\theta_x-\frac{\pi}{2})} e^{i(m-b)\theta} e^{-i(n-a)\theta} W_{n-a,m-b}[B, \sigma, \mu, s\omega] \\ &= \sum_{m,n,a,b\in\mathbb{Z}} \overline{\mathcal{C}_a(z)} e^{-ia(\frac{\pi}{2}-\theta_x)} \mathcal{C}_b(z) e^{im(\frac{\pi}{2}-\theta_\xi)} e^{i(n-a)(\theta_x-\frac{\pi}{2})} e^{i(m-b)\theta} e^{-i(n-a)\theta} W_{n-a,m-b}[B, \sigma, \mu, s\omega] \\ &= \sum_{m',n',a,b\in\mathbb{Z}} \overline{\mathcal{C}_a(z)} e^{-ia(\frac{\pi}{2}-\theta_x)} \mathcal{C}_b(z) e^{-ib(\theta_\xi-\frac{\pi}{2})} e^{im'(\frac{\pi}{2}-\theta_\xi)} e^{in'(\theta_x-\frac{\pi}{2})} e^{im'\theta} e^{-in'\theta} W_{n',m'}[B, \sigma, \mu, s\omega] \end{aligned}$$

https://doi.org/10.1017/S0956792519000160 Published online by Cambridge University Press

$$= \sum_{m',n'\in\mathbb{Z}} e^{i\omega|z|\cos(\theta_\xi-\theta_z)} e^{-i\omega|z|\cos(\theta_x-\theta_z)} e^{im'(\frac{\pi}{2}-\theta_\xi)} e^{in'(\theta_x-\frac{\pi}{2})} e^{i(m'-n')\theta} W_{n',m'}[B,\sigma,\mu,s\omega]$$

$$= \sum_{m',n'\in\mathbb{Z}} \phi_z((\theta_\xi,\theta_x)^T) e^{im'(\frac{\pi}{2}-\theta_\xi)} e^{in'(\theta_x-\frac{\pi}{2})} W_{n',m'}[B^\theta,\sigma,\mu,s\omega]$$

$$= \phi_z((\theta_\xi,\theta_x)^T) A_B^\infty((\theta_\xi-\theta,\theta_x-\theta)^T,\sigma,\mu,s\omega).$$

□

We introduce the descriptor construction based on the far-field pattern [15].

Definition 4.4 Given $\eta=(\theta_\xi,\theta_x)^T$, we define the frequency-dependent *distribution descriptor* of an inhomogeneous object D associated with the permittivity and permeability distributions $\mu(x)$, $\sigma(x)$ as follows:

$$S_D(v;\sigma,\mu,\omega) := \int_{[0,2\pi]^2} |A_D^\infty(\eta;\sigma,\mu,\omega) A_D^\infty(\eta-v;\sigma,\mu,\omega)|\, d\eta. \tag{4.7}$$

The distribution descriptor S_D is invariant to any translation and rotation. More precisely, we can prove the following identity.

Proposition 4.5 *Let $D=z+sR_\theta B$. We have*

$$S_D(v;\sigma,\mu,\omega) = S_B(v;\sigma,\mu,s\omega).$$

Proof Given $\eta=(\eta_1,\eta_2)$, $\theta=(\theta,\theta)$, by $|\phi_z(\cdot)|=1$ and

$$\begin{aligned}\int_{[0,2\pi]^2} A_B^\infty(\eta-\theta;\sigma,\mu,s\omega)\,d\eta &= \int_{[0,2\pi]^2} \sum_{m,n\in\mathbb{Z}} e^{im(\frac{\pi}{2}-(\eta_1-\theta))} e^{in((\eta_2-\theta)-\frac{\pi}{2})} W_{n,m}[B,\sigma,\mu,s\omega]\,d\eta\\ &= \int_{[-\theta,2\pi-\theta]^2} \sum_{m,n\in\mathbb{Z}} e^{im(\frac{\pi}{2}-\eta_1')} e^{in(\eta_2'-\frac{\pi}{2})} W_{n,m}[B,\sigma,\mu,s\omega]\,d\eta'\\ &= \int_{[0,2\pi]^2} \sum_{m,n\in\mathbb{Z}} e^{im(\frac{\pi}{2}-\eta_1')} e^{in(\eta_2'-\frac{\pi}{2})} W_{n,m}[B,\sigma,\mu,s\omega]\,d\eta'\\ &= \int_{[0,2\pi]^2} A_B^\infty(\eta';\sigma,\mu,s\omega)\,d\eta',\end{aligned}$$

we have

$$\begin{aligned}S_D(v;\sigma,\mu,\omega) &= \int_{[0,2\pi]^2} |A_D^\infty(\eta;\sigma,\mu,\omega) A_D^\infty(\eta-v;\sigma,\mu,\omega)|\,d\eta\\ &= \int_{[0,2\pi]^2} |\phi_z(\eta) A_B^\infty(\eta-(\theta,\theta),\sigma,\mu,s\omega)\phi_z(\eta-v) A_B^\infty(\eta-v-(\theta,\theta);\sigma,\mu,s\omega)|\,d\eta\\ &= \int_{[0,2\pi]^2} |A_B^\infty(\eta-(\theta,\theta),\sigma,\mu,s\omega) A_B^\infty(\eta-(\theta,\theta)-v;\sigma,\mu,s\omega)|\,d\eta\\ &= \int_{[0,2\pi]^2} |A_B^\infty(\eta',\sigma,\mu,s\omega) A_B^\infty(\eta'-v;\sigma,\mu,s\omega)|\,d\eta'\\ &= S_B(v,\sigma,\mu,s\omega).\end{aligned}$$

□

https://doi.org/10.1017/S0956792519000160 Published online by Cambridge University Press

5 Numerical experiments

In this section, we present a variety of numerical results in order to demonstrate the applicability of the theoretical framework presented in the previous sections. In particular, we investigate the identification of a target by reconstructing inhomogeneous scattering coefficients from the measurements of the multistatic response (MSR) matrix. In the multistatic configuration, directions of incidence and observations are sampled. For each incident direction, the scattered wave is measured in all the observation directions [10]. The overall procedure verifies the applicability of [15] to the inhomogeneous case. In the following, we study the case of objects with piecewise constant material parameters. For a collection of (inhomogeneous) targets, based on the code developed in [24] for the homogeneous case, we build a frequency-dependent dictionary of distribution descriptors and use a target identification algorithm like the one of [15] to identify an inhomogeneous target from the dictionary up to some translation, rotation and scaling.

The dictionary that we consider is composed by three different groups of objects:

- *Homogeneous targets*, that is, a disk, a triangle, *so on.*
- *Inhomogeneous targets with one inclusion inside*, that is, a circular target with a circular inclusion inside, *so on.*
- *Inhomogeneous targets with two (distinct) inclusions inside*, that is, a circular target with a circular inclusion and a square inside, *so on.*

Note that these inclusions have different material parameters than the ones of the target and the background. The case of a homogeneous target is taken into account in [15]. Finally, we perform numerical experiments in order to test the performance of the scattering coefficients in inhomogeneous target identification.

Given a target D, we proceed as follows:

- *Data simulation*. The MSR matrix is simulated for a frequency range $[\omega_{\min}, \omega_{\max}]$ by evaluating the integral representation (2.8), where the densities are computed by solving (2.7). We adopt a circular acquisition system (a full-view acquisition).
- *Reconstruction of scattering coefficients*. For each frequency, we reconstruct the matrix $\mathbf{W} = (W_{mn}[D^{-z_0}])_{mn}$ of scattering coefficients directly by the formula (3.32) of [15]. A stability analysis of the reconstruction is provided in [15].
- *Target identification*. We calculate the distribution descriptors and use a target identification algorithm; see [15].

5.1 Dictionary

The dictionary $\mathcal{D}$ that we consider is composed by 14 targets (see Figure 1):

- Six elements of the dictionary are homogeneous targets: a disk, an ellipse, a triangle, a square, a rectangle and the letter A. All homogeneous targets share the same permittivity $\mu = 3$ and permeability $\sigma = 3$.
- Five elements of the dictionary are inhomogeneous targets with a single inclusion inside: a disk with a circular inclusion inside, a disk with an ellipse inside, a disk with a triangular inclusion inside, a disk with a square inside and a disk with a rectangular inclusion inside. Note that these five targets share the same permittivity ($\mu_e = 3$) and permeability ($\sigma_e = 3$) for the exterior domain, while all inclusions have permittivity $\mu_i = 6$ and permeability $\sigma_i = 6$.

https://doi.org/10.1017/S0956792519000160 Published online by Cambridge University Press

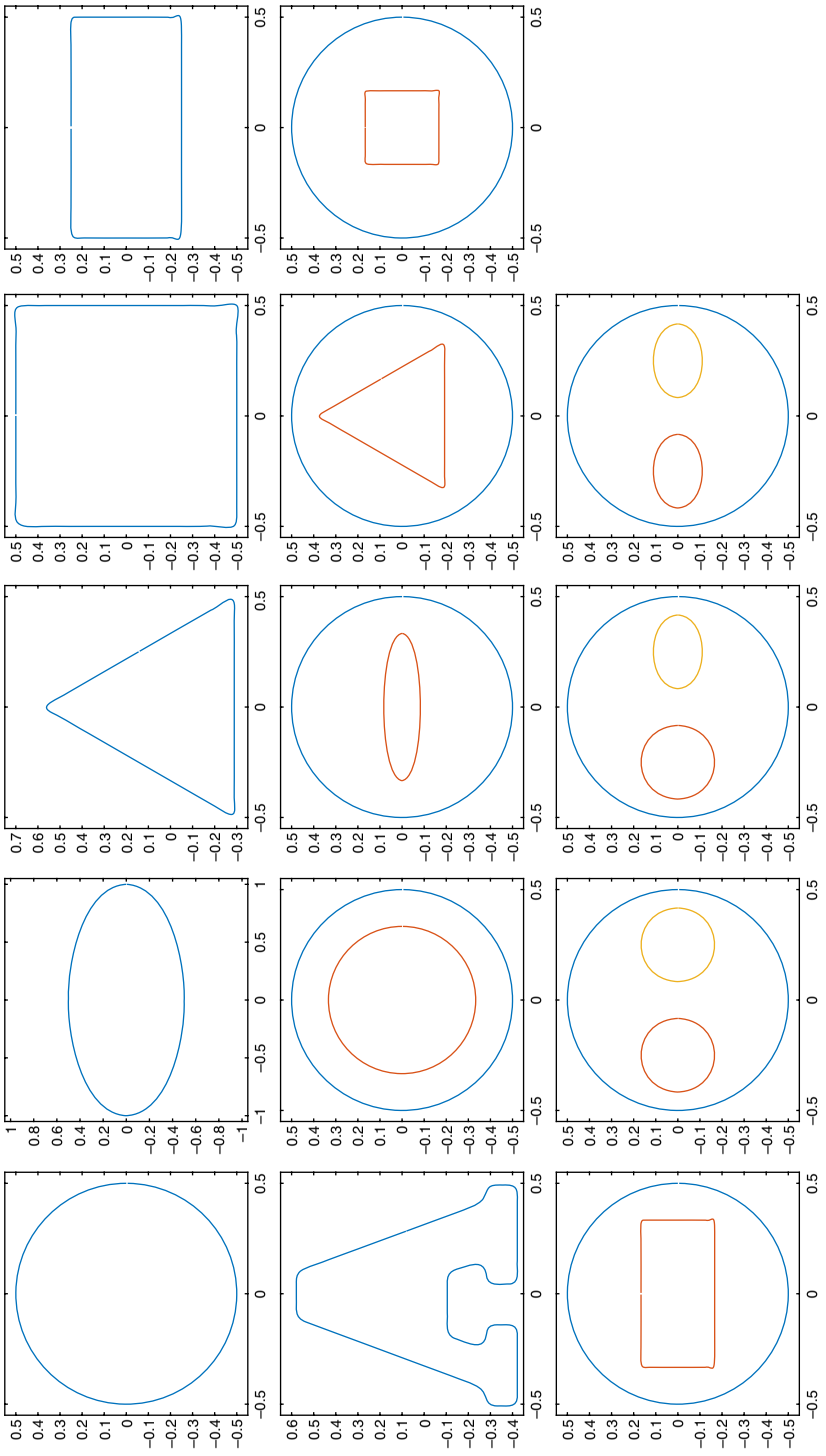


FIGURE 1. Dictionary of targets.

https://doi.org/10.1017/S0956792519000160 Published online by Cambridge University Press

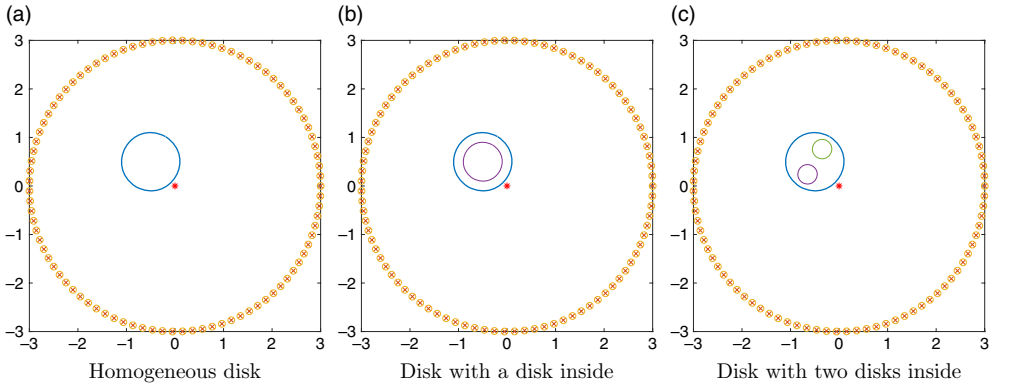


FIGURE 2. Circular acquisition systems for three kinds of targets. We adopt full aperture with $Ns = 91$ plane wave sources (angular position is marked by $\circ$) and $Nr = 91$ receivers (marked by $\times$). Measurement centre is marked by $*$. (a) shows a circular acquisition system for an homogeneous target (a disk); (b) shows a circular acquisition system for an inhomogeneous target (a disk with a circular inclusion inside); (c) shows a circular acquisition system for an inhomogeneous disk with two distinct inclusions inside.

- Three elements of the dictionary are inhomogeneous disks with two distinct inclusions inside: two circular inclusions for the first disk, a circle and an ellipse for the second disk and two distinct ellipses for the third one. These three targets share the same permittivity ($\mu_e = 3$) and permeability ($\sigma_e = 3$) for the exterior domain, while the two distinct inclusions have permittivity $\mu_i = 6$ and permeability $\sigma_i = 6$, $i = 1, 2$.

5.2 Acquisition system

We generate a circular acquisition system using plane waves: the receivers x_r are uniformly distributed on a circle of radius R and centred at z_0, and the sources are plane waves with equally distributed wave direction. More precisely, for the rth receiver we have $|x_r - z_0| = R$ and the angle $\theta_r := \theta_{x_r - z_0} = 2\pi r/N_r$, and the sth plane wave source is given by

$$U_s(x) = e^{ik_0 \xi_s \cdot x},$$

where the vector ξ_s is such that $|\xi_s| = 1$ and $\theta_s := 2\pi s/N_s$. We denote by N_s the total number of plane waves as sources, and by N_r the number of receivers. Note that z_0 can be obtained using some localisation algorithm [10]. Here, we assume that z_0 is close to the centre of the target D.

For this experiment, we adopt a circular acquisition system with $R = 3$, $N_s = 91$ and $N_r = 91$. For simplicity, we always choose the centre $z_0 = [0, 0]^T$. Figure 2 illustrates this acquisition system for the three different elements of the dictionary $\mathcal{D}$.

5.3 Measurements

In each numerical experiment, the unknown target D is obtained from one of the elements of the dictionary by a rotation with angle $\theta = \pi/3$, a scaling $s = 1.2$ and a translation $z = [-0.5, 0.5]^T$. Each element of the dictionary is approximated by 2^9 points.

https://doi.org/10.1017/S0956792519000160 Published online by Cambridge University Press

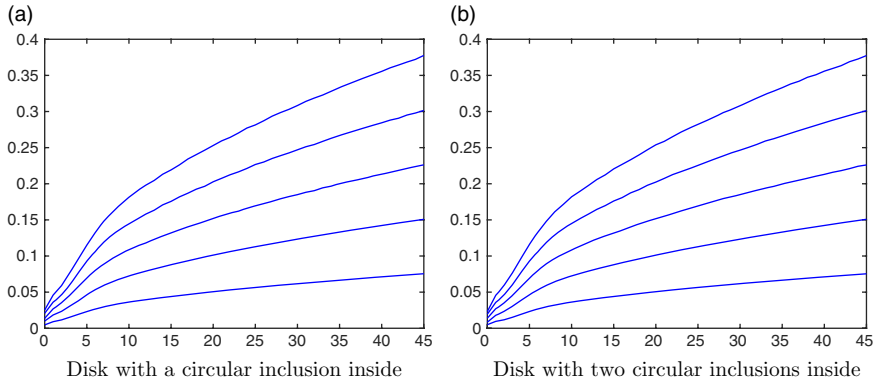


FIGURE 3. Relative error of the reconstruction $\|\mathbf{W}^{\text{est}} - \mathbf{W}\|_F / \|\mathbf{W}\|_F$ for the systems (b) and (c) in Figure 2 at a different order K and fixed frequency $\omega = 0.75\pi$. The curves from bottom to top correspond to percentage of noise $\sigma_0 = 20\%$, 40%, 60%, 80% and 100%. The experiments have been repeated 100 times.

We reconstruct the matrix $\mathbf{W} = (W_{mn})_{mn}$ of scattering coefficients at order $K = 25$. Figure 3 plots the relative error of the (analytical) reconstruction $\|\mathbf{W}^{\text{est}} - \mathbf{W}\|_F / \|\mathbf{W}\|_F$ as a function of K for the three different groups of targets in the dictionary ($\|\cdot\|_F$ denotes the Frobenius norm of matrices). It can be seen that the reconstruction is robust: for example, in the case of a disk with a circular inclusion inside, with 20% of noise, the error is less than 10% for an order K up to 45.

5.4 Scale estimation

Given an unknown target $D_n = z + sR_\theta B_n$ and a dictionary of (inhomogeneous) objects $\mathcal{D} = (B_n)_n$, by measurements we reconstruct the distribution descriptor $S_{D_n}(v; \sigma, \mu, \omega)$ and build a frequency-dependent dictionary of distribution descriptors $(S_{B_n}(v; \sigma, \mu, \omega))_n$, where σ and μ are given.

Note that the distribution descriptor of the target S_{D_n} is frequency dependent. As we proved in the previous sections, since the frequency ω is coupled with the scaling factor s, which is unknown and arbitrary in $(0, \infty)$, to adapt the distribution descriptor S_{D_n} to target identification we assume that the physical operating frequency is limited, that is, $0 < \omega_{\min} \le \omega \le \omega_{\max} < \infty$, and that $0 < s_{\min} \le s \le s_{\max} < \infty$, which means that the target we are interested in should not be too small or too large. Finally, s^{est} can be estimated as in [15] by solving

$$s^{\text{est}} = \arg\min_{s\in[s_{\min},s_{\max}]} \left\{ \int_{\omega_{\min}}^{\omega_{\max}} \left(\int_{[0,2\pi]^2} [S_{D_n}(v; \sigma, \mu, \omega) - S_{B_n}(v; \sigma, \mu, s\omega)] \, \mathrm{d}v \right)^2 \mathrm{d}\omega \right\}. \quad (5.1)$$

Note that a wide range of frequencies $[\omega_{\min}, \omega_{\max}]$ brings more information and therefore improves the estimation (5.1).

5.5 Numerical implementation

We can solve (5.1) by sampling. The overall procedure is similar to the one of [15] for the homogeneous case. Let N_ω^{dic}, N_ω, N_v and N_δ be positive integers. We define:

https://doi.org/10.1017/S0956792519000160 Published online by Cambridge University Press

- $(\omega_l^{\mathrm{dic}})_{l=0,\dots,N_\omega^{\mathrm{dic}}}$ uniformly distributed points on $[\omega_{\min}^{\mathrm{dic}}, \omega_{\max}^{\mathrm{dic}}]$, with $\omega_{\min}^{\mathrm{dic}} := \omega_{\min} s_{\min}$, and $\omega_{\max}^{\mathrm{dic}} := \omega_{\max} s_{\max}$.
- $(\omega_k)_{k=0,\dots,N_\omega}$ uniformly distributed points on $[\omega_{\min}, \omega_{\max}]$.
- $((v_i^1, v_j^2))_{i,j=1,\dots,N_v}$ uniformly distributed points on $[0, 2\pi]^2$.
- $(s_t)_{t=0,\dots,N_\delta}$ uniformly distributed points on $[s_{\min}, s_{\max}]$.
- $I_k(s) := \{1 \le l \le N_\omega^{\mathrm{dic}},$ such that $\omega_{l-1}^{\mathrm{dic}} \le s\omega_k \le \omega_l^{\mathrm{dic}}\}$.

The distribution descriptors S_{B_n} and S_{D_n} are sampled at discrete positions as follows:

$$S_{ijk}^{D_n} := S_{D_n}((v_i^1, v_j^2); \sigma, \mu, \omega_k),\ S_{ijl}^{B_n} := S_{B_n}((v_i^1, \sigma, \mu, v_j^2); \omega_l),$$

where σ and μ are given (see Section 5.1). Finally, we discretise the functional inside the argmin in (5.1):

$$J(t; D_n, B_n) = \sum_{k=0}^{N_\omega} \sum_{l \in I_k(s_t)} \left(\sum_{i,j=1}^{N_v} (S_{ijk}^{D_n} - S_{ijl}^{B_n}) \right)^2,$$

and the scaling factor s^{est} can be estimated by solving

$$\epsilon(D_n, B_n) = \min_{t=0,\dots,N_\delta} J(t; D_n, B_n).$$

5.6 Frequency-dependent dictionary and matching algorithm

We construct the frequency-dependent dictionary of distribution descriptors as follows. For a collection of standard elements of the dictionary $(B_n)_n$, we precompute the discrete samples $(S_{ijl}^{B_n})_{ijl}$ of the distribution descriptor $S_{B_n}(v; \sigma, \mu, \omega)$, for $v \in [0, 2\pi]^2$ and $\omega \in [\omega_{\min}^{\mathrm{dic}}, \omega_{\max}^{\mathrm{dic}}]$. The discrete samples $((S_{ijl}^{B_n})_{ijl})_n$ constitute our frequency-dependent dictionary.

Assume that our (inhomogeneous) target D is generated by an element of the dictionary $(B_n)_n$, up to some unknown translation, rotation and scaling. Suppose that the scaling factor is such that $s_{\min} \le s \le s_{\max}$, where $s_{\min}$ and $s_{\max}$ are known. In order to detect the target D among the elements of the dictionary, we compute the discrete samples $(S_{ijk}^D)_{ijk}$ of the distribution descriptor $S_D(v; \sigma, \mu, \omega)$ and calculate $\epsilon(D, B_n)$ for all elements of the above-mentioned dictionary. The minimiser of $(\epsilon(D, B_n))_n$ is taken as the identified target and is expected to give the best estimation of s^{est}. This procedure is described in detail in Algorithm 1, which was first introduced by Ammari *et al.* [15].

Algorithm 1 Target identification algorithm

Input: $(S_{ijk}^D)_{ijk}$ of unknown target D; $((S_{ijl}^{B_n})_{ijl})_n$ of the whole dictionary.
for B_n in the dictionary **do**
  $\epsilon_n \leftarrow \epsilon(D, B_n)$;
  $n \leftarrow n + 1$;
end for
Output: The true dictionary element $n^* \leftarrow \arg\min_n \epsilon_n$.

https://doi.org/10.1017/S0956792519000160 Published online by Cambridge University Press

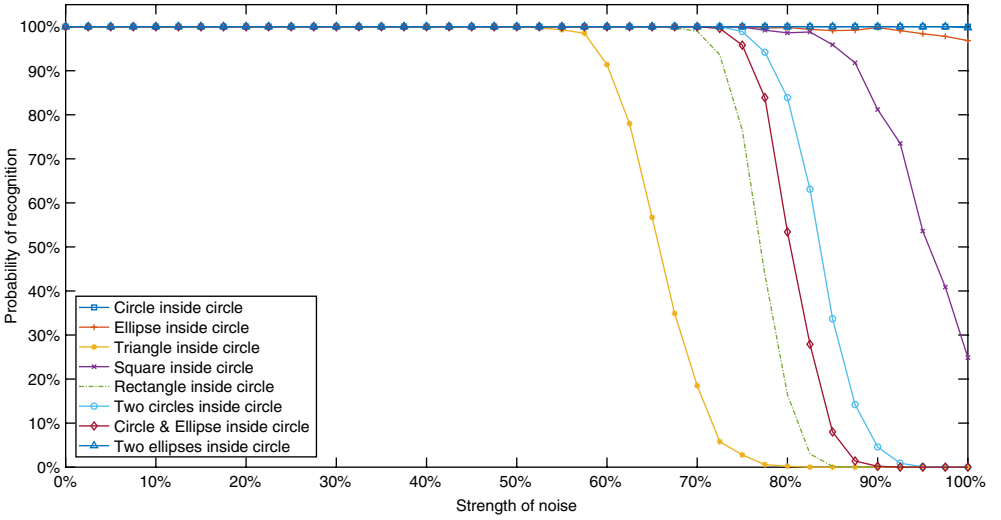


FIGURE 4. Probability of recognition for all inhomogeneous targets of the dictionary of Figure 1 after 1000 independent recognition processes.

5.7 Parameter settings for identification and scaling estimation

For this experiment, the frequency-dependent dictionary of distribution descriptors $((S_{ijl}^{B_n})_{ijl})_n$ is computed for the range of frequency $[\omega_{\min}^{\mathrm{dic}}, \omega_{\max}^{\mathrm{dic}}] = [0.25\pi, 1.5\pi]$, with $N_\omega^{\mathrm{dic}} = 78$ and $N_v = 512$. Data simulation is conducted for the range of operating frequency $[\omega_{\min}, \omega_{\max}] = [0.5\pi, \pi]$ with $N_\omega = 52$. The range of valid scaling factor is $[s_{\min}, s_{\max}] = [0.5, 1.5]$, with $N_\delta = 250$.

5.8 Results of target identification

In this section, we present the main results of target identification obtained using the full-view setting of Figure 2:

- *Separability:* It can be seen that the identification succeeded for all targets with no noise (see Appendix). Notice that the error bars of each identified target have very different numerical value compared to those of the other elements of the dictionary. This means that recognition works well and a dictionary of large size can be used in practice.
- *Probability of recognition:* Figure 4 consists in a complete scheme which depicts the probability of recognition for all inhomogeneous targets of the dictionary at different noise levels. Figure 4 was obtained as follows:

(1) We fixed the level of noise (see x-axis of Figure 4). We selected an inhomogeneous target D to be identified (see the legend). Notice that the target was generated by an element of the dictionary $(B_n)_n$, up to some (unknown) translation, rotation and scaling.
(2) We generated 1000 measurements data for D.
(3) For each measurement, we recovered the scattering coefficients from the data and computed the correspondent distribution descriptor associated to the inhomogeneous target. Notice that the results associated to each computation were different, since our measurements were affected by noise.

https://doi.org/10.1017/S0956792519000160 Published online by Cambridge University Press

(4) We performed the target identification procedure described in detail in Algorithm 1. We calculated the errors $(\epsilon(D, B_n))_n$ between the distribution descriptor of the target returned from noisy measurements and the precomputed distribution descriptors of each element of the dictionary $(B_n)_n$. The minimiser B_{n^*} of $(\epsilon(D, B_n))_n$ was taken as the identified target. If the identified target was correct, we considered the identification successful. Notice that this procedure was repeated for each measurement (1000 in total, corresponding to 1000 realisations of the noise, see (2)).

(5) We computed the number of successful identifications and calculated the probability of success after all the identification procedures. Notice that we reached 100% probability of recognition for the target D if the identified target was classified correctly for each independent target identification procedure (1000 in total, corresponding to 1000 realisations of the noise, see (2)).

(6) Finally, we obtained each line of Figure 4 by repeating (1)–(5) for different levels of noise. Notice that each line corresponds to a different target D (see the legend).

Figure 4 shows that some targets are better identified than others. For example, the target named 'Ellipse inside circle' is very well identified even if the measurements are affected by high levels of noise, while the target 'Triangle inside circle' is confused completely after noise level of 85%. The reason of it cannot be derived entirely by intuition, since our distribution descriptors are complicated functions of the scattering coefficients, which are frequency-dependent geometric quantities that depend also on the electromagnetic properties of the target. Notice that Figure 4 simulated a practical situation, where our data were contaminated by some noise $\mathbf{N}_{\text{noise}}$ where the entries are independent complex Gaussian random variables with mean zero and variance $\sigma^2_{\text{noise}} = \sigma_0 \|\mathbf{V}\|_F/(N_r N_s)$ (σ_0 is the percentage of the noise in the measurement, $\mathbf{V}$ is the MSR matrix). The stronger the noise is, the more it affects the reconstruction of the scattering coefficients (see Figure 3) and the computation of the distribution descriptors. Figure 4 also shows that the overall performance of Algorithm 1, tested for the first time for homogeneous targets in [15], is also good for the inhomogeneous case, since each target is recognised with probability 100% up to a noise level of 50%. Notice that once we reach the threshold of 7.14% probability of detection, a random choice of the object in the dictionary is preferred.

- *Target identification for* $\sigma_0 = 40\%$*:* Figure 5 shows the average error bars for all inhomogeneous targets with noise $\sigma_0 = 40\%$. Figure 5 was obtained as follows:

(1) We fixed the level of noise $\sigma_0 = 40\%$. We selected an inhomogeneous target to be identified (see x-axis of Figure 5) among all the targets $(D_n)_n$. Notice that the target was generated by an inhomogeneous element of the dictionary $(B_n)_n$, up to some (unknown) translation, rotation and scaling. In the following, we consider to apply the target identification procedure to D_1, that is, the target generated by the inhomogeneous element of the dictionary B_1 ('Circle inside circle', see x-axis of Figure 5) up to some (unknown) translation, rotation and scaling.

(2) We generated 1000 measurements data for D_1.

(3) For each measurement, we recovered the scattering coefficients from the data and computed the correspondent distribution descriptor associated to the inhomogeneous target D_1. Notice that the results associated to each computation were different, since our measurements were affected by noise.

https://doi.org/10.1017/S0956792519000160 Published online by Cambridge University Press

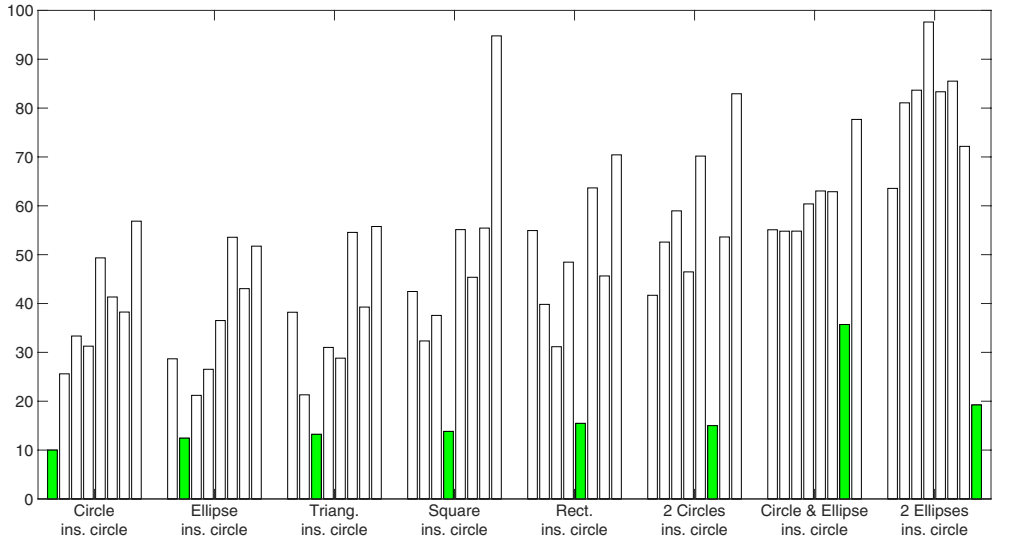


FIGURE 5. Average error bars after 1000 independent recognition processes for all inhomogeneous objects in the full-view setting and $\sigma_0 = 40\%$. Since the probability of recognition is 100% for all inhomogeneous targets with noise $\sigma_0 = 40\%$, the shortest bar in each group is also the target identified by the matching procedure.

(4) We calculated the errors $(\epsilon(D_1, B_n))_n$ between the distribution descriptor of the target D_1 returned from noisy measurements and the precomputed distribution descriptors of all the inhomogeneous elements of the dictionary $(B_n)_n$ (see x-axis of Figure 5). The errors were memorised inside a vector $\mathbf{E}_1 = (\epsilon(D_1, B_1), \epsilon(D_1, B_2), ...)$.

(5) We repeated (3) and (4) for each measurement data. This resulted in 1000 vectors $\mathbf{E}_1$, $\mathbf{E}_2$, ..., $\mathbf{E}_{1000}$ of errors (corresponding to 1000 realisations of the noise).

(6) We computed the average error vector $\mathbb{E}_1$ between $\mathbf{E}_1$, $\mathbf{E}_2$, ... $\mathbf{E}_{1000}$. Notice that the mth component of $\mathbb{E}_1$ corresponds to the average error between the distribution descriptor of D_1 and the precomputed distribution descriptor of the mth inhomogeneous element of the dictionary. Notice that the average error is calculated over 1000 realisations of $\epsilon(D_1, B_m)$.

(7) We repeated (1)–(6) for each inhomogeneous target of the dictionary. We obtained the vectors $\mathbb{E}_1$, $\mathbb{E}_2$,..., with $\mathbb{E}_n$ being the average of the errors between the inhomogeneous target D_n and the inhomogeneous elements of the dictionary.

Figure 5 is composed by eight groups of bars. The nth group corresponds to the inhomogeneous target D_n (see the x-axis legend of Figure 5) generated by the correspondent inhomogeneous element of the dictionary B_n up to some (unknown) translation, rotation and scaling. Each group is composed by eight error bars. The mth error bar of the nth group corresponds to the mth component of $\mathbb{E}_n$, that is the average of the errors resulting from the matching experiment for D_n using the element of the dictionary B_m. For each group, the shortest bar indicates the lowest average error and is marked in green. In this case, since Figure 4 shows that the probability of recognition is 100% for all inhomogeneous targets with noise $\sigma_0 = 40\%$ (i.e., each recognition process is successful), the shortest bar in each group also

https://doi.org/10.1017/S0956792519000160 Published online by Cambridge University Press

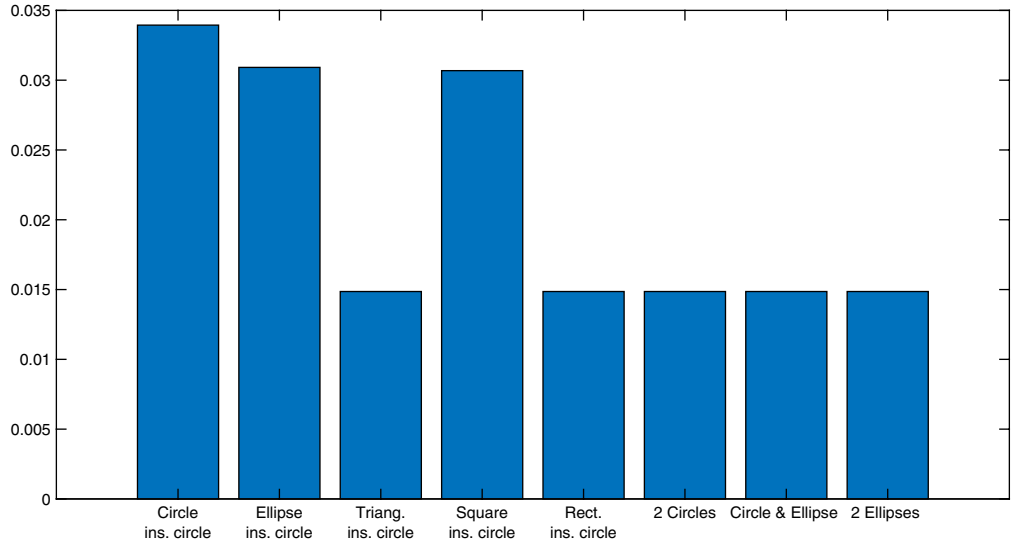


FIGURE 6. Average difference between the estimated scaling factor and the true one (s = 1.2) at $\sigma_0 = 40\%$ after 1000 independent recognition processes.

identifies the correct target. For $\sigma_0 = 40\%$, the estimated scaling factor s^{est} is also close to the true value $s = 1.2$; see Figure 6.

6 Concluding remarks

In this paper, we have presented a framework of target identification for inhomogeneous objects. We have provided and numerically tested in the presence of measurement noise a procedure for target classification in wave imaging based on matching on a dictionary of precomputed frequency-dependent distribution descriptors. The construction of such frequency-dependent distribution descriptors is based on the properties of the inhomogeneous scattering coefficients. For a collection of inhomogeneous targets, we first extracted the scattering coefficients from the reflected waves and then used a target identification algorithm in order to identify an inhomogeneous target from the dictionary up to some translation, rotation and scaling. It can be seen that the identification succeeded for all targets with noise σ_0 up to 50%.

Appendix. Target identification with $\sigma_0 = 0\%$

We present results of target identification obtained using the full-view setting of Figure 2 with no noise ($\sigma_0 = 0\%$). The computation of the error $\epsilon(D, B_m)$ is represented by error bars in Figure A1, where the mth error bar in the nth figure corresponds to the error $\epsilon(D, B_m)$ of the matching experiment using the generating element of the dictionary B_n for the target. Since there is no noise, the shortest bar in each group is the identified target. As expected, the identification succeeded for all targets.

https://doi.org/10.1017/S0956792519000160 Published online by Cambridge University Press

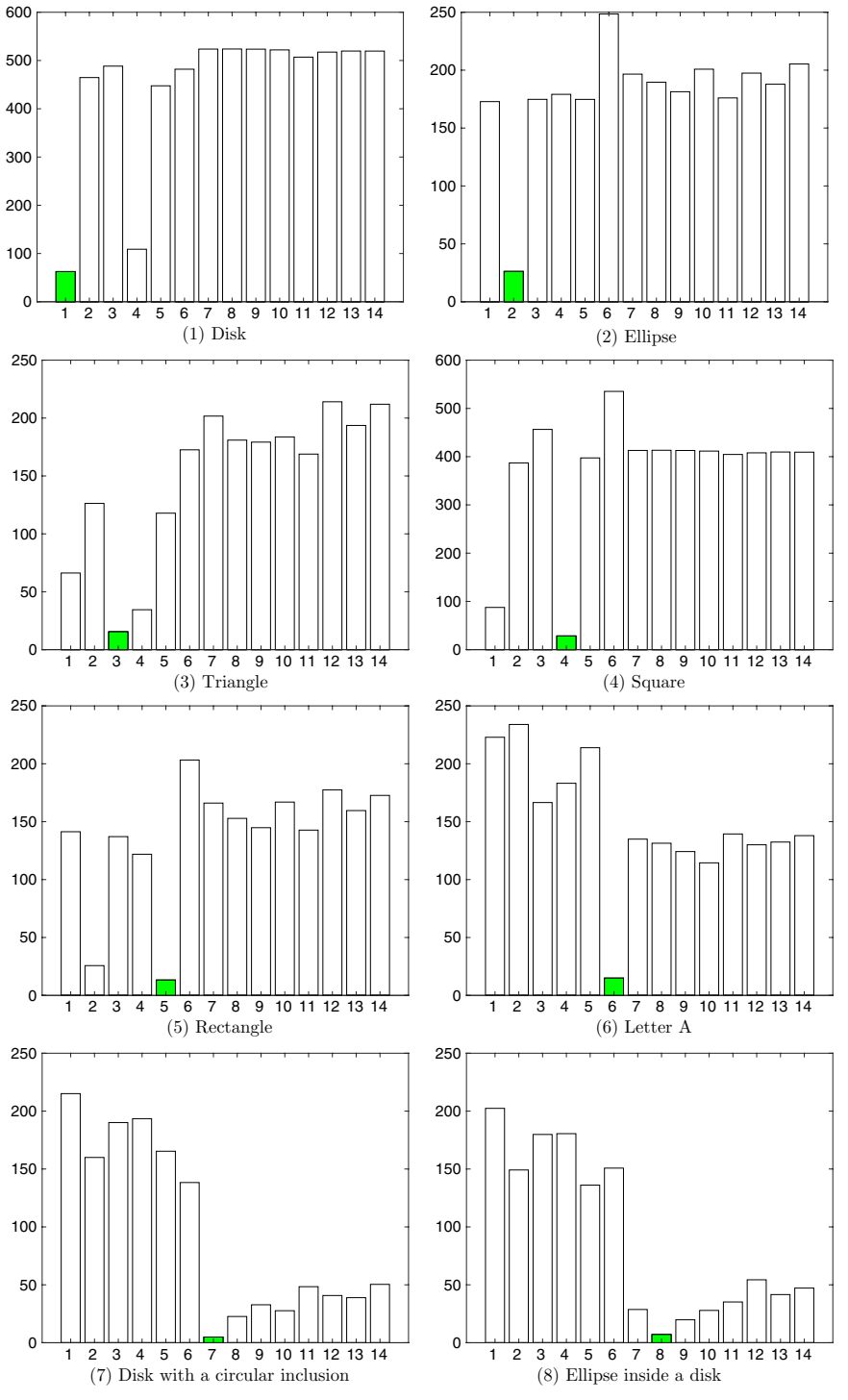


FIGURE A1. Results of identification for all elements of the dictionary in the full view and no noise.

https://doi.org/10.1017/S0956792519000160 Published online by Cambridge University Press

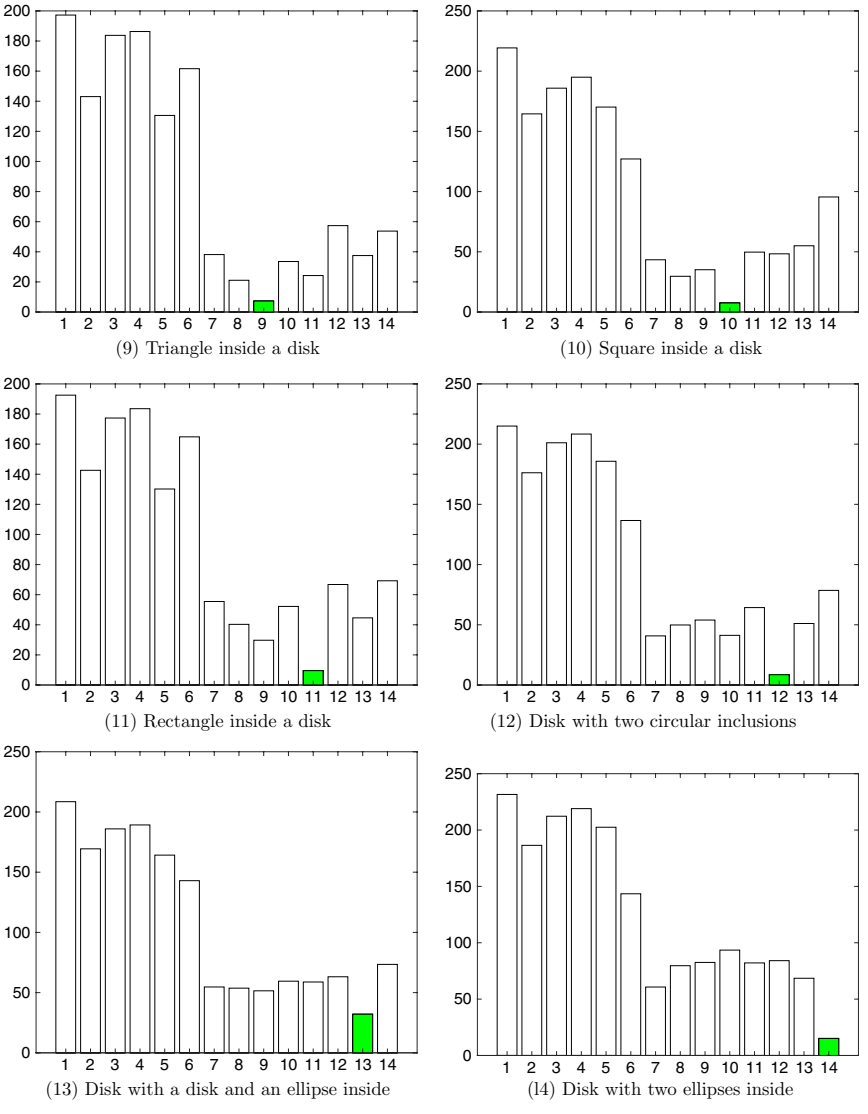


FIGURE A1. (Continued)

Acknowledgements

The author gratefully acknowledges Prof. H. Ammari for his guidance and would like to thank the referees for their valuable comments. During the preparation of this work, the author was financially supported by a Swiss National Science Foundation grant (number 200021-172483).

Conflict of interest

None.

https://doi.org/10.1017/S0956792519000160 Published online by Cambridge University Press

References

[1] ABBAS, T., AMMARI, H., HU, G., WAHAB, A. & YE, J.CH. (2017) Elastic scattering coefficients and enhancement of nearly elastic cloaking. *J. Elast.* **128**, 203–243.

[2] ABRAMOWITZ, M. & STEGUN, I. (1964) *Handbook of Mathematical Functions with Formulas, Graphs, and Mathematical Tables*, National Bureau of Standards Applied Mathematics Series, Vol. 55, Dover, New York.

[3] AMMARI, H., BOULIER, T. & GARNIER, J. (2014) Shape recognition and classification in electro-sensing. *Proceedings of the National Academy of Sciences USA* **111**, 11652–11657.

[4] AMMARI, H., BOULIER, T., GARNIER, J., JING, W., KANG, H. & WANG, H. (2014) Target identification using dictionary matching of generalized polarization tensors. *Found. Comput. Math.* **14**, 27–62.

[5] AMMARI, H., CHOW, Y. T. & ZOU, J. (2014) The concept of heterogeneous scattering coefficients and its application in inverse medium scattering. *SIAM J. Math. Anal.* **46**, 2905–2935.

[6] AMMARI, H., CHOW, Y. T. & ZOU, J. (2014) *The concept of heterogeneous scattering coefficients and its application in inverse medium scattering*, preprint, arXiv:1310.6096, 2013.

[7] AMMARI, H., CHOW, Y. T. & ZOU, J. (2016) Phased and phaseless domain reconstruction in inverse scattering problem via scattering coefficients. *SIAM J. Appl. Math.* **76**, 1000–1030.

[8] AMMARI, H., CHOW, Y. T. & ZOU, J. (2018) Super-resolution in imaging high contrast targets from the perspective of scattering coefficients. *J. Math. Pures Appl.* **111**, 191–226.

[9] AMMARI, H., DENG, Y., KANG, H. & LEE, H. (2014) Reconstruction of inhomogeneous conductivities via generalized polarization tensors. *Ann. IHP Anal. Non Lin.* **31**, 877–897.

[10] AMMARI, H., GARNIER, J., JING, W., KANG, H., LIM, M., SØLNA, M. & WANG, G. (2013) *Mathematical and Statistical Methods for Multistatic Imaging*, Springer, Cham, Switzerland.

[11] AMMARI, H. & KANG, H. (2004) Boundary layer techniques for solving the Helmholtz equation in the presence of small inhomogeneities. *J. Math. Anal. Appl.* **296**, 190–208.

[12] AMMARI, H., KANG & H., LEE (2009) *Layer potential techniques in spectral analysis*, Mathematical Surveys and Monographs, vol. 153, American Mathematical Society, Providence, RI. MR2488135

[13] AMMARI, H., KANG, H., LEE, H. & LIM, M. (2013) Enhancement of Near-Cloaking. Part II: The Helmholtz Equation. *Comm. Math. Phys.* **317**, 485–502.

[14] AMMARI, H., GARNIER, J., JUGNON, V., LEE, H. & LIM, M. (2012) Enhancement of near-cloaking. Part III: Numerical simulations, statistical stability, and related questions. In: *Multi-scale and High-Contrast PDE: from Modelling, to Mathematical Analysis, to Inversion*, Contemp. Math., Vol. 577, Amer. Math. Soc., Providence, RI, pp. 1–24.

[15] AMMARI, H., TRAN, M. P. & WANG, H. (2014) Shape identification and classification in echolocation. *SIAM J. Imaging Sci.* **7**, 1883–1905.

[16] AMMARI, H., KANG, H., KIM, E. & LEE, J.-Y. (2012) The generalized polarization tensors for resolved imaging. Part II: Shape and electromagnetic parameters reconstruction of an electromagnetic inclusion from multistatic measurements. *Math. Comp.* **81**, 839–860.

[17] AMMARI, H., FITZPATRICK, B., KANG, H., RUIZ, M., YU, S. & ZHANG, H. (2018) *Mathematical and computational methods in photonics and phononics*, Mathematical Surveys and Monographs, Vol. 235, Amer, Math. Soc., Providence.

[18] COLTON, D. & KRESS, R. (1992) *Inverse Acoustic and Electromagnetic Scattering Theory*. Applied Math. Sciences, Vol. 93, Springer-Verlag, New York.

[19] KLEEMAN, L. & KUC, R. (1995) Mobile robot sonar for target localization and classification. *Internat. J. Robotics Res.* **14**, 295–318.

[20] NÉDÉLEC, J. C. (1992) Quelques propriétés des dérivées logarithmiques des fonctions de Hankel. *C. R. Acad. Sci. Paris, Série I* **314**, 507–510.

[21] PÓLYA, G. & SZEGÖ, G. (1951) *Isoperimetric Inequalities in Mathematical Physics*, Ann. Math. Stud. Vol. 27, Princeton University Press, Princeton, NJ.

[22] SIMMONS, J. A. (1979) Perception of echo phase information in bat sonar. *Science* **204**, 1336–1338.

[23] SIMMONS, J. A., FENTON, M. B. & O'FARRELL, M. J. (1979) Echolocation and pursuit of prey by bats. *Science* **203**, 16–21.

[24] WANG, H. (2014) *Shape identification in electro-sensing*, https://github.com/yanncalec/SIES

https://doi.org/10.1017/S0956792519000160 Published online by Cambridge University Press